ResearchGate

See discussions, stats, and author profiles for this publication at: https://www.researchgate.net/publication/349414064

The influence of heat transfer due to radiation heat transfer from a combustion chamber

Article *in* Journal of Thermal Analysis and Calorimetry · February 2021

DOI: 10.1007/s10973-020-10263-3

CITATIONS
11

READS
427

4 authors, including:

Ahmad Reza Ravangard
Old Dominion University

3 PUBLICATIONS **21** CITATIONS

SEE PROFILE

Ladan Momayez
University of Pittsburgh

31 PUBLICATIONS **280** CITATIONS

SEE PROFILE

All content following this page was uploaded by Ladan Momayez on 15 January 2024.

The user has requested enhancement of the downloaded file.

Journal of Thermal Analysis and Calorimetry
https://doi.org/10.1007/s10973-020-10263-3

The influence of heat transfer due to radiation heat transfer from a combustion chamber

Babak Razmjooei[1] · **Ahmad Reza Ravangard**[2] · **Ladan Momayez**[3] · **Mohsen Ferchichi**[3]

Received: 4 February 2020 / Accepted: 15 September 2020
© Akadémiai Kiadó, Budapest, Hungary 2021

Abstract
Combustion process in industrial furnaces remains a challenging research subject. To achieve a realistic model and analyze the influences of heat transfer due to radiation in a combustion process, various phenomena must be examined, such as the hydrodynamic properties of the fuel, two-phase turbulent flow, and chemical reactions, which occur in the turbulent environment. A proper study of the processes mentioned above leads to the correct analysis of the process and a reduction of emissions and the homogeneous temperature, and more importantly, it helps to reduce fuel consumption. This research has solved combustion equations by the flame-let and Arrhenius one-step equation model, and also heat transfer due to radiation mechanism by the Discrete Ordinates Method (DOM) equations with a gray gas hypothesis. Modeling is based on OpenFoam software, and results are validated with previous works. Results show that changes in water vapor and carbon dioxide concentration lead to change in heat transfer due to radiation, and the combustion process of oxygen with an extra percentage will radically reduce the chamber temperature compared to the combustion with air. By assuming the gray gas hypothesis, the effects of radiation heat transfer on gas and wall heat flux are between 10% to 68% and 10% to 40%, respectively. This work matches the experimental results more accurately than previously reported models.

REVISED PROOF

Keywords Discrete Ordinates Method (DOM) · Combustion · Radiation heat transfer · Gray gas · Turbulence · Heat flux

List of symbols

a_k	Stoichiometric coefficient of reactants
a_g	Emission weigh factor for WSGG model
a_s	Absorption weigh factor for WSGG model
a_ε	Summation of thermal weigh factor for WSGG model
$b_{\varepsilon.i.j}$	Weigh factor for WSGG model
b_k	Stoichiometric coefficient of products
C_p	Specific heat coefficient
C_μ	Constant turbulence coefficient
$C_{\varepsilon 1}$	Constant turbulence coefficient
$C_{\varepsilon 2}$	Constant turbulence coefficient
c	The coefficient of WSGG model
D	Mass diffusion coefficient (m^2/s)
dn_k	Mole fraction variation (mol)
E_{φ_i}	The lower state energy of the line
e	Internal energy (J)
g	Specific external force (m/s^2)
h_p	Planck constant
h	Enthalpy (kJ/kg)
I	Total energy (J)
J	Mass flux ($kg\ s^{-1}\ m^{-2}$)
K	Boltzmann constant
$\mathcal{K}$	Thermal conductivity coefficient (W/mK)
k	Species index
L	Radiation path length (m)
MR	Molar concentration (mole)
m_φ	Total number of absorption coefficients
N	Total number of species
P_t	The total pressure of the mixture (atm)
PL	Pressure per length (atm m)
p	Pressure (atm)
q	Heat flux (W/m^2)
Q	Internal partition function of the molecule
$\dot{Q}$	The rate of heat production (W/s)
R	Reaction rate (mol/m^2s)
S	The intensity of the spectral line

✉ Ladan Momayez
Ladan.momayez@google.com

[1] Department of Mechanical Engineering, Shahid Bahonar University, Kerman, Iran

[2] Department of Aerospace Engineering, University of Tehran, Tehran, Iran

[3] Department of Mechanical and Aerospace Engineering, Royal Military College of Canada, Kingston, ON K7K 7B4, Canada

Journal : Large 10973 | Article No : 10263 | Pages : 18 | MS Code : 10263 | Dispatch : 24-1-2021

$\overline{S_{ij}}$	Strain rate tensor (s^{-1})
T	Temperature (K)
$\widetilde{T}$	Average temperature (K)
T_g	Gas temperature (K)
T_{ref}	Reference temperature (K)
t	Time (s)
u	Velocity (m/s)
$\overline{u_j u_j}$	Sub-grid scale Reynolds shear stress (N m^{-2})
V	Stoichiometric coefficient of chemical component
V'	Stoichiometric coefficient of chemical component reactant
V''	Stoichiometric coefficient of chemical component product
W_k	Weight factor of species k
$\dot{w}_k$	The average rate of reaction (mol/s)
$\dot{w}_T$	The average work of turbulent dissipation (J)
X	Chemical symbol
x	Spatial components (m)
Y	Mass fraction
$\widetilde{Y}$	The average molar mass of components (mol)
z	Mixing ratio

Greek letters

ζ_{φ}^{i}	Linear absorption coefficients
φ	Spectral line location (cm^{-1})
Φ	The ratio of oxidizer to fuel
γ	The broadening property of the spectral line
κ	Gray gas coefficient
η	Minimum length scale (m)
ε	Dissipation rate (m^2/s^3)
υ	Kinematic viscosity (m^2/s)
χ	Scalar dissipation rate
ε_g	Gas emission coefficient
λ	Second viscosity coefficient (Pa s)
μ_B	Bulk viscosity/first viscosity coefficient (Pa s)
μ	Dynamic viscosity (Pa s)
μ_t	Turbulent viscosity (kg/m s)
δ	Kronecker function
τ	Viscous stress tensor (Pa)
ρ	Density (kg/m^3)
σ	Prandtl number

Introduction

Industrial furnaces are known to consume large amounts of energy. Thus, from an environmental and economic standpoint, research and investment in furnace energy consumption are critical. The recent stringent environmental regulations have motivated both academics and industries to develop strategies to evaluate energy utilization to minimize energy losses, to reduce pollutants emission, etc. Despite the large volume of literature on combustion processes in industrial furnaces, the complexity arising from emissions and absorption of radiation during combustion is not yet well documented.

Dependence of emission and absorption coefficient on temperature, pressure along optimal path length, radiative emission wavelength, and chemical species concentrations, make analytical solution difficult. The most accurate methods for modeling the radiation field in the chamber are the Zone Method and the Monte Carlo Method. Fernandes and Francis [1] used Galerkin finite element method and Crank-Nicolson scheme in order to handle interpolation procedure and transient terms, respectively, for a combined conduction and radiation problem with the presence of absorption, emission, and saturation in an entirely gray cylindrical medium. They showed that the compatibility of finite element techniques with the variable integral limits could help evaluate conduction fluxes. Smith et al. [2] introduced modifications to the dominant coefficients in the gray model for cases such as carbon dioxide, water vapor, and their mixture, which resulted in more applicable collections of coefficients for temperature and pressure per length (PL) within the range from 600 to 2400 K and 0.001 to 10.0 atm m, respectively. However, for the lower values of these two variables, the results differed from the measurements.

Joo et al. [3] experimentally utilized a thermo-phoretic soot sampling system inside a high-pressure chamber comprising the ethylene–air laminar diffusion flame. Soot samples were gathered by transmission electron microscope grids at three heights over the burner rim normally, 3 mm, 8 mm, and 12 mm. In their investigation, the images captured by the electron microscope indicated the mean initial soot particle diameter increased from the sampling height of 3 mm to 8 mm at the mid-height of the flames where the peak soot volume fractions are detected. The soot diameters decreased from the mid-height of the flame to the sampling location of 12 mm, close to the edge of the flame. The mean diameter of the initial soot particle increased with increasing pressure up to 15 bar; then, at 20 bar, the mean soot diameter seemed to reach a plateau, after which it dropped monotonically.

Lallemant et al. [4] conducted several investigations on the limitations of applying total emissivity correlations in computational fluid dynamics (CFD) computer codes for disposed modeling of flame behavior. In their research, several models total emissivity prediction for H_2O–CO_2 mixture were compared with the Exponential Wide-Band Model (EWBM) computations. Using a coupled approach in which the property models and the radiative transfer equation (RTE) were solved, they surveyed the correlating methodology performances on non-homogeneous applications, especially for combustion in a chamber. In their study, a variety of different models, such as the total transmittance, non-homogeneous model (TTNH), the spectral group model

REVISED PROOF

Journal : Large 10973	Article No : 10263	Pages : 18	MS Code : 10263	Dispatch : 24-1-2021

(SGM), and the combined five gray gas model (WSGG), were applied and compared. Their work showed value, that a remarkable deviation of vapor to carbon dioxide partial pressure from the expected complete combustion of methane and air.

Modest and Zhang [5] developed and accurate, efficient full-spectrum correlation-k distribution for radiative transfer calculations from which the popular WSGG model originated. Despite the model limitations, all the essential characteristics of heat transfer in a furnace, such as gray walls, gray scattering, are included, and it provided accurate evaluation. A gas mixture comprising carbon dioxide and nitrogen was studied by considering a scaling approximation that offered a significantly efficient evolution of radiative heat flux. Their results demonstrated the applicability of using the WSGG method for both gray enclosures and other scattering media.

Li and Modest [6] studied the turbulence–radiation interactions (TRI) effects using a composition probability density function (PDF) in the case of a methane/air diffusion flame glazing in a combustion chamber. Their study showed that by ignoring TRI, the radiative heat loss is always underestimated and, therefore, temperature levels are mostly overestimated. They indicated for determination of TRI, absorption coefficient–Planck function correlation has nonlinear relation to temperature and is more critical than other correlations and needs to be calculated precisely.

Han [7] has performed investigations on a pyrolyzing fuel ignition and flame propagation, in which the two-dimensional unsteady model was employed as well. According to the presented data, the gas radiation in the low over-heat ratio resulted in a weak blue flame at a uniform mixture temperature. They indicated as the over-heat ratio was raised to 3, the steady visible blue flames appear and self-propagated despite the degrees of gas contribution.

Chen [8] conducted a one-dimensional numerical evaluation of flame propagation near stoichiometric methane and air mixture. With the help of adaptive mesh refinement, Chen [8] simulated the spherical flame propagation up to a radius of 4 m inside a sizeable computational domain of 20 m. He showed that, for the near stoichiometric methane/air mixture, radiation had a slight influence on small-scale spherical flame propagation with radius below 4 cm while both radiative loss and radiation absorption had a significant impact on large-scale spherical flame propagation with radius up to 4 m, his experiments have shown that the acceleration parameter is not affected by radiation absorption. He found when radiation absorptions ignored, radiation effects have an overestimated effect on acceleration exponent. Since in experiments for large-scale spherical flame propagation, radiation due to radiation absorption has a minor impact on the acceleration exponent.

Wall et al. [9] studied three types of coals in furnaces experimentally and numerically. They estimated the effect of heat transfer due to radiation on the gas properties and the recycling of outgoing carbon dioxide. They showed that radiation could impose changes on gas properties and their heat capacity. Hjärtstam et al. [10] presented a numerical approach to gas analysis and soot-related radiation mechanism for an oxy-fuel flame. They reported that the presence of soot radiation had a more prominent role than the radiative properties. Ben-Mansour et al. [11] considered a cylindrical reactor wall. They showed that speed, temperature, species concentration, and heat flux are the basic parameters in heat transfer due to the radiation process. They also predicted the combustion characteristics for a variety of gas mixtures through which the importance of the amount of CH_4 on the combustion process was confirmed. Centeno et al. [12] assessed a turbulent non-premixed flame in a cylindrical chamber in which the WSGG model achieved a radiation field. In their study, the standard $k-\varepsilon$ model was selected to calculate the turbulence field for this particular kind of flame. The results showed the vital role of capturing radiation characteristics in the interaction between the flame and radiation.

Kou [13] reported a collection of radiation and other related concepts for heat transfer considerations that are predominantly used in this study. Marshall et al. [14] developed a computational code for numerical validation of experiments within a spherical vessel comprising injection, ignition, and other essential instruments for measurement. The overall outline of his study showed an acceptable validation between numerical and empirical analysis. Experimental visualization of a turbulent flame of premixed and non-premixed methane sprayed into a chamber was recorded in novel research presented by Cavaliere et al. [15]. The results can be useful for making a comparison between numerical methods, like large eddy simulation, and it could be beneficial to capture validations of this kind of combustion for a profound understanding of turbulence impact on other desired different aspects, including radiation impact on combustion characteristics. Turns [16] published an exhaustive collection on combustion behavior for different situations, which can be used for additional development in later studies.

Leckner [17] compiled a variety of essential characteristics of water vapor and carbon dioxide for heat transfer radiation in an infrared spectrum in order to provide an understanding of spectral and total emissivity charts of water vapor and carbon dioxide. Calculations were compared to the available spectral data from different sources in which a 10% contrast was reported. Yin et al. [18] modified the WSGG model for a high precision computation. They examined the uncertainty of different models according to their applicability and validity. Through the presented study, a viable database for air–fuel and oxy–fuel

REVISED PROOF

Journal : Large 10973	Article No : 10263	Pages : 18	MS Code : 10263	Dispatch : 24-1-2021

was derived, which surprisingly was used for two distinct beam lengths in a furnace heat transfer simulation.

The line by line (LBL) model, proven to be an accurate model in radiation, has a spectral database that possesses over 60 radiative transitions and is definite by high-temperature gas simulation, and so capturing radiative transitions is feasible. Despite its accuracy for radiation heat transfer, it is time-consuming and expensive for many simulations, and this has limited the use of this model. Bordbar et al. [19] employed this model for radiation modeling for inhomogeneous media, and the result showed the remarkable accuracy of the LBL model. A novel developed data collection of spectrometry analysis for gas molecules at high temperature (HI-TEMP) was presented by Rothman et al. [20], which is practical for industrial applications. Their study includes a group of common species in combustion phenomena such as H_2O, OH, CO, CO_2, and NO.

Rivière et al. [21] developed an approximate spectroscopic database for H_2O, which applies for the lowest level of energy to the highest state of rotation or molecular vibration motion in which component of water molecules has the highest rate of emission. Considering the fact that a combustion process includes the interaction between different species, and also wave emission of each species inside the chamber, the spectral studies accomplished in the literature provide researchers valuable database for measurements. Rivière et al. [21] used an extrapolation analysis on existing various spectral databases and LBL analysis to achieve more precise information in the higher level of energy. Based on this endeavor, narrow-band model parameters for H_2O emissions, which were statistically derived times ago, have been efficiently developed.

CHU et al. [22] have recently represented two narrow-band models for gas radiation in a specific planar geometry containing two different types of mixtures. In the first case, they assessed a mixture with CO_2 and the other one without CO_2 at the standard thermodynamic condition. This study includes different models, such as the Goody SNB model [23] and the Malkmus SNB model [24]. A comparison between these two models accomplished by these researchers showed the former model is preferred for engineering applications.

Toporov et al. [25] experimentally studied an oxy-coal flame, and the published results were well organized as a benchmark for validating numerical models. Similar approach is also used in [26–28].

Ravangard et al. [29] examined a multiphase–multicomponent model utilizing the Lattice Boltzmann method. Their investigation compares two models through which multiphase and multicomponent phenomena such as combustion could be modeled. Müller et al. [30] realized a steady laminar flame-let model for non-premixed combustion by the use of turbulence models such as LES and RANS. They used reliable numerical options and compared the results with other experimental investigations, and showed good agreement and proved the capability of the new implementation to model turbulent combustion at a reasonable computational effort.

Li et al. [31] studied a method based on the control volume finite element for nanofluid MHD natural convective flow under the impact of thermal radiation, in which the effect of magnetic field on thermal radiation was examined. They showed the increase of buoyancy forces on the inner wall temperature reduction and the decrease in convective heat transfer. Sheikholeslami et al. [32] investigated the effect of using CuO nanoparticles on thermal behavior and considered radiative terms in their simulations. Their results demonstrate that minimum solidification time has been obtained for Platelet shape, and solid faction improves with the increase in radiation parameter. Research conducted by Sheikholeslami et al. [33] confirms the importance of some factors affecting the energy variation in a turbulent flow inside a pipe equipped with innovative turbulators. They showed that exergy drop decreases with enhancing Reynolds number and height ratio. Second law performance increases with enhancement of height ratio while it decreases with enhancement of pitch ratio.

A complimentary thermal algorithm beside a hydrodynamic-based solver might be a well-manner new strategy for heat transfer evaluation in either complex geometries or the complex interface between species in combustion modeling. It should be noted that developing a radiation model must be considered for radiation evaluation.

There is no doubt that scientific and environmental agencies recognize the importance of designing better combustion chambers such as dangerous emission and pollution are maintained at that safe level, and in reducing its large energy consumption, a better understanding of the many factors that affect the performance of combustion chamber can be helpful to analyze the impact of emission on heat transfer, and also lowering potential effects of radiation on the device efficiencies.

Here, we benefit from theoretical models such as the flame-let model to assess various factors and their effects on fuel consumption reduction. Factors like water vapor and carbon dioxide concentration, and the type of oxidizer introduced into the chamber (pure oxygen or air) can extremely determine whether radiation and other factors with can reduce the temperature inside the combustor. Temperature variation during the combustion process provides designers a remarkable valuable informations for optimizing device performance and reducing the harmful effect of improper combustion inside the chambers and its directly related impacts on environmental protection.

Combustion simulation by the use of numerical methods plays a significant role in the low-cost examination of different

REVISED PROOF

Journal : Large 10973	Article No : 10263	Pages : 18	MS Code : 10263	Dispatch : 24-1-2021

industrial devices. OpenFOAM which is an advanced numerical tool, may be considered the high-performance simulation software. This current work benefits OpenFOAM open-source code, which provides authors with a variety of combustion models such as XiFoam, SprayEngineFoam, and reactingFoam. The open foam allows us to include additional model equations into the code depending on the selected problem condition.

Governing equations

The analysis of chemically reacting flows is described by a fundamental principles such as the conservation of mass, momentum, energy and chemical reaction. Accurate assessment of thermodynamic and heat transfer in the flow field requires the use of turbulence and radiation models.

Continuity and momentum equations

The total mass of the system does not change for all flows be-it passive or reactive species either convert to other. The conservation of mass equation in these flows is express as:

$$\frac{\partial \rho}{\partial t} + \frac{\partial}{\partial x_i}\left(\rho u_i\right) = 0, \tag{1}$$

while the differential momentum equation is giving as:

$$\frac{\partial}{\partial t}\left(\rho u_i\right) + \frac{\partial}{\partial x_j}\left(\rho u_i u_j\right) = -\frac{\partial p}{\partial x_i} + \frac{\partial \tau_{ij}}{\partial x_j} + \rho \sum_{k=1}^{N} Y_k g_{k,i}. \tag{2}$$

where ρ is the density, u_i is the mean velocity in x direction, p is the pressure, the expression $g_{\mathrm{K}i}$ implies the specific force, and Y_k is the mass fraction of species k from N species that exist in the reaction. By considering the Newtonian fluid, the viscous stress tensor τ_{ij} is proportional to velocity gradient (i.e., the time rate of strain):

$$\tau_{ij} = \mu\left(\frac{\partial u_i}{\partial x_j} + \frac{\partial u_j}{\partial x_i}\right) + \left(\mu_\mathrm{B} - \frac{2}{3}\mu\right)\frac{\partial u_k}{\partial x_k}\delta_{ij}. \tag{3}$$

where the Kronecker function δ_{ij} which has the value of 1 (when $i = j$) and 0 (when $i \neq j$). The term $\mu_\mathrm{B} - {}^2/_3\mu$ is called second viscosity coefficient (λ), μ_B is the bulk viscosity (or first viscosity coefficient), and μ is the dynamic viscosity coefficient. According to the Stokes' hypothesis the value of λ and μ_B is defined $-\frac{2}{3}\mu$ and 0, respectively. Both of λ and μ_B are dependent on pressure and temperature variations.

Energy equation

The law of conservation of energy expresses the concept of unchanged total energy in an isolated system. According to the definition, the total energy of a system is stated as the contribution of mechanical and thermal energies. By considering the algebraic expressions of each type of energies, the final form of energy equation is given as below:

$$\frac{\partial}{\partial t}(\rho I) + \frac{\partial}{\partial x_j}\left(\rho I u_j\right) = -\frac{\partial q_j}{\partial x_j} - \dot{Q} - \frac{\partial}{\partial x_j}\left(p u_j\right) + \frac{\partial}{\partial x_j}\left(\tau_{ij} u_i\right) + \rho \sum_{k=1}^{N} Y_k g_{k,i}\left(u_i + V_{k,i}\right). \tag{4}$$

where the sum of internal energy and kinetic energy is expressed as the total energy I,

$$I = e + \frac{1}{2}u_i u_i. \tag{5}$$

$\dot{Q}$ is the rate of heat production and the heat flux is as below:

$$q_\mathrm{j} = \mathcal{K}\frac{\partial T}{\partial x_\mathrm{j}} + \rho \sum_{k=1}^{N} h_\mathrm{k} Y_\mathrm{k} V_\mathrm{k,i}, \tag{6}$$

where $\mathcal{K}$ is thermal conductivity coefficient, T is the temperature, and the enthalpy of the species k is h_k. The first term on the right of Eq. (6), which is called Fourier's law, introduces the heat diffusion effects, while the second term shows the heat diffusion of different components with different enthalpies.

An equation of state establishes a relationship among pressure, temperature, and density of the gas, and it is essential to specify all of the terms of the stress tensor. In this work, the ideal gas model was considered, and specific enthalpy of the chemical species and the specific heat values is obtained by Janaf [13]. The following equation of state, which is practical for homogenous mixtures, and other factors, such as specific heat and enthalpy, are extracted from Janaf tables:

$$p = R_0 T \sum_{k=1}^{N}\left(\frac{\rho_\mathrm{k}}{W_\mathrm{k}}\right), \tag{7}$$

$$C_\mathrm{p}(T) = \sum_{k=1}^{N}\left(\frac{\rho_\mathrm{k}}{\rho}\right) C_\mathrm{p,k}(T), \tag{8}$$

$$h_\mathrm{k}(T) = I_\mathrm{k}(T) + \frac{R_0 T}{W_\mathrm{k}}, \tag{9}$$

where $R_0 = 8315\ \frac{\mathrm{J}}{\mathrm{kmol\ K}}$ that is the universal gas constant, W_k is weight factor that represents the ratio of mass fraction to molecular weight for species k, and C_p is specific heat coefficient in constant pressure.

REVISED PROOF

Journal : Large 10973	Article No : 10263	Pages : 18	MS Code : 10263	Dispatch : 24-1-2021

The chemical species conservation equation

In flows that species are produced and consumed at a certain rate in a way that the mass of each species may confront may be changing, but the total mass of reacting mixture remains constant and conserved. This statement can be expressed as:

$$\frac{\partial}{\partial t}\left(\rho Y_{\mathrm{k}}\right) + \frac{\partial}{\partial x_{\mathrm{j}}}\left(\rho Y_{\mathrm{k}} u_{\mathrm{j}}\right) = \frac{\partial\left(-J_{\mathrm{k,j}}\right)}{\partial x_{\mathrm{j}}} + R_{\mathrm{k}}, k = 1, \ldots, N, \quad (10)$$

where Y_{k} is the mass fraction, J is the mass flux in x_{j} direction, and R_{k} is the reaction rate. Fick's law represents the direct relationship between the mass flux and the concentration gradient, and by neglecting the Soret effect and pressure diffusion, the final expression can be written as $J_{\mathrm{k,j}} = \rho D_{\mathrm{k}} \frac{\partial Y_{\mathrm{k}}}{\partial x_{\mathrm{j}}}$ that D_{k} is diffusion coefficient of species k. The combustion process is considered as a chemical reaction in which stoichiometric rules are defined as:

$$\sum_{k=1}^{N} a_{\mathrm{k}} X_{\mathrm{k}} \leftrightarrow \sum_{k=1}^{N} b_{\mathrm{k}} X_{\mathrm{k}}, \quad k = 1, \ldots, N, \quad (11)$$

where a_{k} and b_{k} are stoichiometric coefficients for backward and forward reaction, and X_{k} represents the chemical symbol of the species k. Because the total mass during all reaction is conserved, the algebraic addition of stoichiometric coefficients for both sides of the chemical reaction equation is equal to zero, i.e., $\sum_{k=1}^{N}\left(a_{\mathrm{k}} - b_{\mathrm{k}}\right) W_{\mathrm{k}} = 0$, which means the consumption of specific element results in the production of the element on the right-hand side of the equation (the ordinary concepts of stoichiometric equilibrium from chemistry). As the combustion phenomenon is a kind of chemical reaction that burns substances and produces heat, the burning reaction is directly proportional to the portion of the generated heat in the combustion chamber that leads to the definition of burn rate as $\frac{d\varepsilon}{dt} = \left(V_{\mathrm{k}}'' - V_{\mathrm{k}}'\right)\frac{dn_{\mathrm{k}}}{dt}$ [13, 14].

Turbulence

Only two phenomena control combustion: chemical reactions and mixing (i.e., transport of energy, species, and momentum). A Reynolds Averaged Navier–Stokes (RANS) turbulence model is usually employed to justify the increased mixing as a result of the presence of turbulence in fluid flow. The addition of a turbulent viscosity not only increases mixing, but it also ignores smaller scales in the CFD simulation. The turbulent viscosity excludes smaller scales; however, it is common for RANS engine combustion simulations to be insufficiently resolved. The non-existence of a sufficient sub-grid term needs to be modeled. In the situation of combustion simulation, it is shown that often virgule, this sub-grid term is considerably more important than Turbulent Chemistry Interaction terms (TCI). It is also shown that by adding sufficient mesh resolution to a RANS simulation, accurate combustion results can be achieved by using precise chemistry directly. One of the vital parameters which have a considerable effect on the development process and optimization of fuel consumption is turbulence. Turbulence leads to a premium mixing of fuel and air, and to creating combustion with favorable conditions. Fluid flow is called turbulent when all transfer values such as mass, momentum, and energy have irregular fluctuations in space and time periodically. Under these circumstances, mixing improves the transition variables [15, 16].

The presence of large eddies in turbulent flows is characterized over a wide range of length and time scales. The size of eddies may vary from large scale to microscale that are the integral length scales (L) and (η), the Kolmogorov microscales. When large eddies successively break into small eddies, the overall kinetic energy must be equal to the energy dissipation. These smallest eddies are correct wise by Kolmogorov length scales. The Kolmogorov microscales are defined as $\eta \approx \left(\frac{\nu^3}{\varepsilon}\right)^{1/4}$, $\tau \approx \left(\frac{\nu}{\varepsilon}\right)^{1/2}$ and $u_\eta \approx (\nu\varepsilon)^{1/4}$, ε is dissipation rate. The characteristic microscales are Kolmogorov length scale, viscous microscale and velocity microscale. When the Reynolds number increased, the separation between the integral and Kolmogorov scales also increases.

Reynolds decompositions and averaging of the conservation equation where employed in this work. Reynolds decomposition consists of expressing an instantaneous property ϕ as the sum of the mean time average and a fluctuation ϕ' as $\phi(t) = \overline{\phi} + \phi'(t)$. According to the presented definition, the mean value of ϕ within the average time interval is expressed as below:

$$\overline{\phi} = \frac{1}{\Delta t}\int_{t-\frac{1}{2}\Delta t}^{t+\frac{1}{2}\Delta t} \phi(t)\mathrm{d}t = \frac{1}{T}\int_{0}^{T} \phi(t)\mathrm{d}T \quad (12)$$

In combustion, the density is variable; the mass-weighted averaging is used in some variables in principle conservation equations. This method divides the quantity into a mean value $\tilde{\phi}$ and a fluctuation value ϕ'', and can be written as $\phi(t) = \tilde{\phi} + \phi''(t)$, where $\tilde{\phi} = \frac{\overline{\rho\phi}}{\overline{\rho}}$. Using the above decomposition the conservations equations become:

$$\frac{\partial\overline{\rho}}{\partial t} + \frac{\partial}{\partial x_i}\left(\overline{\rho}\tilde{u}_i\right) = 0, \quad (13)$$

$$\frac{\partial}{\partial t}\left(\overline{\rho}\tilde{u}_i\right) + \frac{\partial}{\partial x_j}\left(\rho\tilde{u}_i\tilde{u}_j\right) = -\frac{\partial\overline{p}}{\partial x_i} + \frac{\partial}{\partial x_j}\left(\overline{\tau_{ij}} - \overline{\rho u_i' u_j'}\right) + \overline{\rho g_i}, \quad (14)$$

REVISED PROOF

Journal : Large 10973 | Article No : 10263 | Pages : 18 | MS Code : 10263 | Dispatch : 24-1-2021

$$\frac{\partial}{\partial t}\left(\bar{\rho}\tilde{h}\right) + \frac{\partial}{\partial x_j}\left(\bar{\rho}\tilde{h}\tilde{u}_j\right) = \frac{\overline{Dp}}{Dt} + \frac{\partial}{\partial x_j}\left(\bar{\rho}D_k\frac{\partial\tilde{h}}{\partial x_j} - \bar{\rho}\widetilde{u_j''h''}\right) + \bar{Q} + \overline{S_\mathrm{h}}, \tag{15}$$

$$\frac{\partial}{\partial t}\left(\bar{\rho}\widetilde{Y}_\mathrm{k}\right) + \frac{\partial}{\partial x_j}\left(\bar{\rho}\widetilde{u}_j\widetilde{Y}_\mathrm{k}\right) = \frac{\partial}{\partial x_j}\left(\bar{\rho}D_\mathrm{k}\frac{\partial\widetilde{Y}_\mathrm{k}}{\partial x_j}\right) - \frac{\partial}{\partial x_j}\left(\bar{\rho}\widetilde{u_j''Y_j''}\right) + \overline{R_k}, \tag{16}$$

where S_h is the source term which represents the losses due to friction and R_k is the rate of consumption or production by any mechanism inside the control volume. In order to model the Reynolds stresses and other unsolved terms such as enthalpy and turbulent fluxes related to chemical species, these terms can be closed by considering a gradient-diffusion hypothesis and Boussinesq hypothesis by performing algebraic operations leads to the following final equation for RNS turbulence model:

$$\frac{\partial}{\partial t}\left(\bar{\rho}k\right) + \frac{\partial}{\partial x_j}\left(\bar{\rho}\widetilde{u}_j\kappa\right) = \frac{\partial}{\partial x_j}\left[\left(\mu + \frac{\mu_\mathrm{t}}{\sigma_\kappa}\right)\frac{\partial\kappa}{\partial x_j}\right] + P_\kappa - \bar{\rho}\varepsilon, \tag{17}$$

$$\frac{\partial}{\partial t}\left(\bar{\rho}\varepsilon\right) + \frac{\partial}{\partial x_j}\left(\bar{\rho}\widetilde{u}_j\varepsilon\right) = \frac{\partial}{\partial x_j}\left[\left(\mu + \frac{\mu_\mathrm{t}}{\sigma_\varepsilon}\right)\frac{\partial\varepsilon}{\partial x_j}\right] + C_{\varepsilon 1}\frac{\varepsilon}{\kappa}P_\kappa - C_{\varepsilon 2}\bar{\rho}\frac{\varepsilon^2}{\kappa}, \tag{18}$$

where the turbulence viscosity can be written as $\mu_t = C_\mu\bar{\rho}\frac{\kappa^2}{\varepsilon}$, σ_κ is the turbulent Prandtl number for the turbulent energy κ_j, σ_ε is the Prandtl number for the dissipation of the turbulence energy ε. P_κ is the source term that can be determined by the Boussinesq approximation.

Large eddy simulation is a well established numerical method for solving fluid flow. In such a model, the large vortices simulation is based on solving and modeling small motion. The averaged momentum and transfer equations lead to nonlinear terms of $\overline{u_j\varphi}$ and $\overline{u_j u_j}$ which cannot be either separated or solved directly. These terms, which are the Reynolds stress and scalar flux, respectively, are written as $\overline{u_j u_j} = \overline{u}_i\overline{u}_j + \tau_{ij}$ and $\overline{u_j\varphi} = \overline{u}_i\overline{\varphi} + q_{ij}$. By using the Smagorinsky model, the term in the momentum equation known as the Reynolds stresses is $\tau_{ij} = \overline{u_j u_j} - \overline{u}_i\overline{u}_j$, and the Reynolds term would be given as $\tau_{ij} = -2\vartheta_t\overline{S}_{ij}$, where parameters ϑ_t, $\overline{S}_{ij}$ and τ_{ij}, respectively, are the vortex viscosity, strain rate tensor, and Reynolds stress. The strain rate tensor is expressed as follows [16]:

$$\overline{S_{ij}} = \frac{1}{2}\left(\frac{\partial\overline{u_i}}{\partial x_j} + \frac{\partial\overline{u_j}}{\partial x_i}\right). \tag{19}$$

Combustion

In this research, parameters such as species mass fraction and temperature properties variation after combustion are achieved by several processes. In this research statistical mechanics and kinetic theorem are two methods that capture the fluid motions from a statistical view point. By defining the probability density function (PDF) as the main factor for the definition of existing particles with specific energy and momentum within the computational domain, each of random variables is set to a value which defines its relative probability [34].

This method can be divided into two models are equilibrium and the flame-let, in which two important issues can be considered separately in each of them. First, the flame structure, measured by its average mass, $\widetilde{Y}_\mathrm{k}$, the average temperature, $\widetilde{T}$, the average response rate, $\dot{w}_\mathrm{k}$, are expressed as a function of the mixing ratio of z. Second, mixing is measured by its average mixing ratio $\tilde{z}(x_i, t)$ [32].

Flame-let model

The flame-let approach can be considered as an extension of the "flame sheet" model, which assumes infinitely fast chemical reaction such that the reaction zone is an infinitely thin interface. With the identical diffusivity assumption in constant pressure combustion without heat loss, the thermo-chemical properties are determined by the local mixing state, which is defined by the mixture fraction. The flame-let approach reduces the considerably fast chemistry assumption by introducing the scalar dissipation rate as a parameter to describe the degree of departure from the equilibrium state. However, the flame-let method still relies on the hypothesis that the time scales for chemical kinetics are much shorter than time scales of convection and diffusion. Under this condition of generally separated time scales, the combustion chemistry reaches a quasi-steady-state and adjusts immediately to the local flow condition.

In the flame-let model, the flame is embedded as small elements in the turbulent flow, so it is structured as a laminar flame. The described laminar flame structures are also usable for calculating the turbulent flame elements. According to this assumption, the whole combustion area needs to be much thinner than the turbulent flow scales. According to these hypotheses, the flame structure is given by the functions $\widetilde{Y}_\mathrm{k}$ and $\widetilde{T}$ which are calculated using Eqs. (20) and (21) given as [32]:

$$\rho\frac{\partial\widetilde{Y}_\mathrm{k}}{\partial t} = \dot{w}_\mathrm{k} + \rho D\left[\frac{\partial z}{\partial x_i}\frac{\partial z}{\partial x_j}\right]\frac{\partial^2\widetilde{Y}_\mathrm{k}}{\partial z^2} = \dot{w}_\mathrm{k} + \frac{1}{2}\rho\chi\frac{\partial^2\widetilde{Y}_\mathrm{k}}{\partial z^2}, \tag{20}$$

where the scalar dissipation rate is:

$$\chi = 2D\left[\frac{\partial z}{\partial x_i}\frac{\partial z}{\partial x_j}\right]. \tag{21}$$

REVISED PROOF

Journal : Large 10973 | Article No : 10263 | Pages : 18 | MS Code : 10263 | Dispatch : 24-1-2021

Substituting temperature T into Eq. (20), then the temperature equation is derived as:

$$\rho \frac{\partial T}{\partial t} = \dot{w}_{\mathrm{T}} + \frac{1}{2} \rho \chi \frac{\partial^2 T}{\partial z^2}, \tag{22}$$

where $\widetilde{Y}_{\mathrm{k}}$ and $\widetilde{T}$ may be calculated for the specific points on the flame, which is independent of turbulence, and stored in the flame-let library. The average mass ratio of components and the temperature [31] can be written by consideration for premixed combustion condition and added a variable density to these equations as:

$$\overline{\rho}\widetilde{Y}_{\mathrm{k}} = \int_0^{+\infty} \int_0^1 \rho Y_{\mathrm{k}}\left(z, \chi_{\mathrm{st}}\right) p\left(z, \chi_{\mathrm{st}}\right) \mathrm{d}z \mathrm{d}\chi_{\mathrm{st}}, \tag{23}$$

$$\overline{\rho}\widetilde{T} = \int_0^{+\infty} \int_0^1 \rho T\left(z, \chi_{\mathrm{st}}\right) p\left(z, \chi_{\mathrm{st}}\right) \mathrm{d}z \mathrm{d}\chi_{\mathrm{st}}. \tag{24}$$

and the probability density function of the weighted average is:

$$\rho p\left(z, \chi_{\mathrm{st}}\right) = \overline{\rho}\widetilde{p}(z) p\left(\chi_{\mathrm{st}}\right). \tag{25}$$

The probability density function for mixing ratio z and scalar losses rate χ_{st} is initialized as the first step of calculations. A similar scenario for initializing the Dirac delta function is used, which allows the calculation of the static scalar dissipation rate and this setting by guarantying the unchanged rate of scalar dissipation across the flame front provide well-defined initial conditions for solving the mentioned equations [13].

Radiation heat transfer modeling

Combustion products include non-gray gases such as water vapor and carbon dioxide. Gary gas assumption in calculations makes operations related to real gases easier. Equations for the radiation modeling of gray gases in a typical chamber are, in a way, organized so that they can be applied for a system containing real gases by choosing a correct range of relating constants in the mentioned equations. Thus, the presented methodology would be practical for various types of gases.

WSGG model

In this method, the wavelength range is separated into several active wavelength ranges and a transparent range. According to Eqs. (26) and (27), it is only dependent on gas temperature

$$\varepsilon_{\mathrm{g}} = \sum_{i=0}^{n} a_{g,i}\left(1 - e^{-\kappa_{g,i} \cdot \mathrm{PL}}\right), \tag{26}$$

$$\alpha_{g \cdot s} = \sum_{i=0}^{n} a_{s,i}\left(1 - e^{-\kappa_{g,i} \cdot \mathrm{PL}}\right), \tag{27}$$

$$a_{\varepsilon \cdot i} = \sum_{j=1}^{N_g} b_{\varepsilon,i,j} T_{\mathrm{g}}^{j-1}. \tag{28}$$

where parameters are gas emission coefficient (ε_{g}), weigh factors for WSGG model ($a_{g,i}$, $a_{\varepsilon.i}$, $a_{s,i}$, $\alpha_{g,s}$), gray gas coefficient ($\kappa_{g,i}$), the partial pressure of species (P), and radiation path length (L). These relations lead to the following equation:

$$\sum_{i=1}^{N_g} a_{\varepsilon,N}\left(T_{\mathrm{g}}\right) = 1, \tag{29}$$

All of the coefficients in Eqs. (26) to (29) are as the form given in [18].

Line by line model

The line by line (LBL) model is considered as one of the most accurate models in radiation heat transfer modeling. The LBL initially calculates the linear absorption coefficients in which the higher quantity of spectrums results in a higher level of precision and much more CPU time. Equation (30) shows this step of the calculation:

$$\zeta_{\varphi}^{i} = \frac{S_i}{\pi} \frac{\gamma_i}{\gamma_i^2 + \left(\varphi - \varphi_i\right)^2}, \tag{30}$$

where ζ_{φ}^{i} and φ are linear absorption coefficients and spectral line locations, respectively. Additionally, the intensity of the spectral line (S_i) is introduced through Eq. (31) that this definition relies on some of the inherent physical parameters such as $S_{\mathrm{ref}.i}$ (the reference value for intensity of spectral line), T_{ref} (the reference temperature), Q (internal partition function of molecules) and E_{φ_i} (the lowest state of energy)

$$S_i = S_{\mathrm{ref},i} \frac{Q\left(T_{\mathrm{ref}}\right)}{Q(T)} \frac{e^{\left(\frac{-E_{\varphi_i}}{KT}\right)}}{e^{\left(\frac{-E_{\varphi_i}}{KT_{\mathrm{ref}}}\right)}} \frac{\left[1 - e^{\left(\frac{-h_p c \varphi_i}{KT}\right)}\right]}{\left[1 - e^{\left(\frac{-h_p c \varphi_i}{KT_{\mathrm{ref}}}\right)}\right]}, \tag{31}$$

that in this equation the broadening property of the spectral line (γ_i) and the total linear absorption coefficient (ζ) can be expressed as the following equations:

$$\gamma_i = \left(\frac{T_{\mathrm{ref}}}{T}\right)^n \left[\gamma_{\mathrm{air}}\left(P_{\mathrm{T}} - P_{\mathrm{s}}\right) + \gamma_{\mathrm{self}} P_{\mathrm{S}}\right], \tag{32}$$

REVISED PROOF

$$\zeta_\varphi = \sum_i \zeta_\varphi^i. \tag{33}$$

For simplicity, we used air instead of oxygen, and the reference temperature of 298 K up to 1000 K. The products' chemical reaction, CO_2, and water vapor were the dominant constituents. Calculating the nonlinear intensity of spectral line and the nonlinear spectral line location is very expensive and time-consuming, the simplified Eq. (28) is used a coherence value of $\Delta\varphi = 0.025\ \mathrm{cm}^{-1}$. In this research, the results for the LBL model were calculated for a water concentration of 2.0, and ε and ζ_j are the emission coefficient and the total linear absorption coefficient [19–21].

$$\varepsilon = \frac{1}{KT^4} \sum_{j=1}^{m_\varphi} E_\varphi\left(1 - e^{-\zeta_j L}\right). \tag{34}$$

Problem description

Boundary conditions and initial values are given in Table 1. In this study, the process of burning methane has been studied in which methane and oxygen are a mixture with a stoichiometric ratio of 0.6. According to the general reaction equation below, methane is considered as the main fuel, oxygen plays the role of oxidizer agent, and the products are carbon dioxide and water:

$$a\mathrm{CH_4} + b(\mathrm{O_2} + 0.78\ \mathrm{N_2}) \rightarrow c\mathrm{CO_2} + d\ \mathrm{H_2O},$$

where a, b, c and d are stoichiometric coefficients of this reaction. The settings are arranged in a way that the flame burning velocity remains 0.135 m/s.

Figure 1 shows the geometry and significant dimensions (0.5 m × 3 m) and total frame time as $t = 0.60$ s at the combustion chamber. The number of nodes used in the numerical solution was 1.086570×10^6, which is achieved from the grid study shown in Fig. 2. The grids were refined close to the walls shear layers, then the mesh refinement is relaxed, and grid size became more abundant along to the chamber. The geometry of Fig. 1 is separated into two regions. The first zone, ($0<x<2$) in which the flame is modeled in this zone, and heat transfer due to radiation is not included, and the second zone, ($2<x<3$), that there are the methane and oxygen in this zone. The flame geometry analyzed in the first zone. In the second zone, there is no flame, but the gas produced during the combustion, and the radiation heat transfer are just modeled and solved for the gas. The priority for both reducing simulation time and increasing the precision of solving problems should be considered by grid refinement. Here, four grids resolution is introduced that shows the grid refinement has been considered for efficient computer cost management and precision achievement.

Table 1 Boundary conditions and initial values

Type of fuel	Methane
Oxidizer	Air/oxygen
ϕ	0.6
Pressure input	1 atmosphere
Velocity Input	13.3 m/s
Temperature input	300 K
Bottom wall temperature	300 K
Top wall temperature	570 K
φ	0.65
Flame burning velocity	0.135 m/s
Maximum Courant number	0.48

Figure 3 illustrates the independence of the grid achieved to solve this problem. In this figure, grid A has 8.14750×10^5 nodes and B, C, and D have one, two, and three million nodes, respectively. This figure has been plotted for 2 min of stimulation, and after that, all three curves coincide. The number of nodes used for the numerical solution is 1.086570×10^6. Since we need to use a series of knots and plate matrices in the CFD procedure, the used mesh has more nodes compared to grid B.

The boundary condition at the walls such that the side walls and bottom walls where at 300 K and the top wall was at 570 K. At the injection point, the mixture of methane and oxygen enters the domain at the velocity of 13.3 m/s where the atmospheric pressure is considered 1 atm, and the condition for the exit boundary is pressure outlet at 1 atm.

Results and discussion

In this research, the whole process of combustion (initial condition to final point) has been numerically simulated. The evolution of combustion for different times is shown in Fig. 4. The two-dimensional computational domain was considered for the fluid flow simulation. Time marching progress of combustion and the corresponding velocity vectors are shown in Figs. 4 and 5, respectively. The flame has different shapes in changing times. The presented results show the effects of flame instability and moving combustion throughout the chamber. These figures show the variation of heat flux via the time which as showing in the Fig. 5. After starting the combustion, and the flam developed longitudinally, then it experienced instabilities—and ultimately reached a relatively steady state condition.

REVISED PROOF

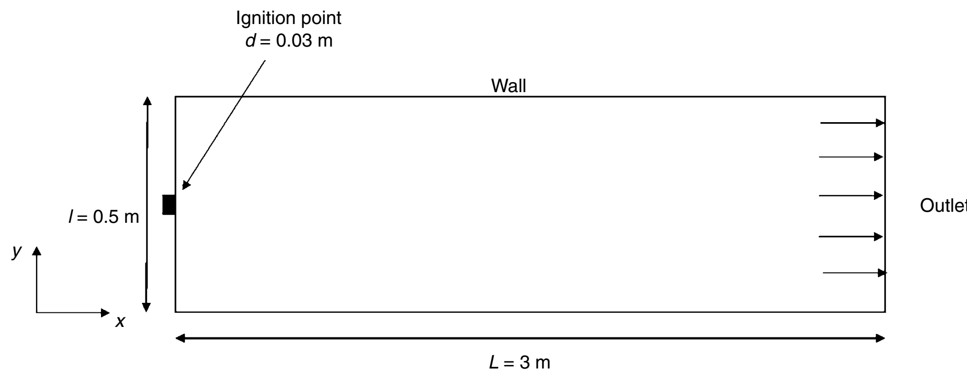

Fig. 1 The schematic diagram of the considered geometry

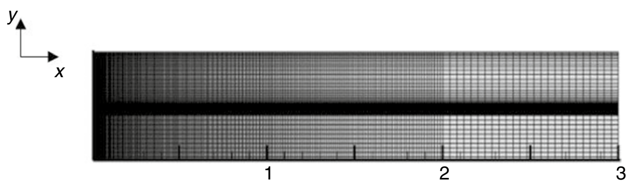

Fig. 2 The generated structured mesh in the computational domain

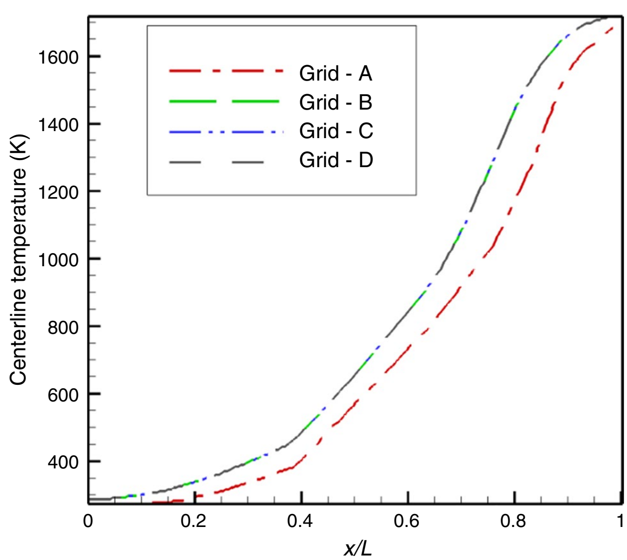

Fig. 3 Grid study results for centerline temperature profile

Figures 6 and 7 show the variation of axial velocity versus longitudinal distance for different turbulence models is in better agreement. As it is indicated in Fig. 6 and Fig. 7, the RANS model is in better agreement with Toporov [25] results compare to LES results of the chamber close to the inlet, while for the entire combustion chamber, where transition conditions are damped, the LES turbulence model shows better agreement with Toporove [25]. Based on these results, the LES model was selected for this study. Due to the existence of multiple subroutines in the LES model, LES has more oscillation, and the convergence is achieved at longer time is due to the use of the Smagorinsky method, and the model attempting to correct itself in each sweep. As it is indicated in figures the RANS model is in better agreement compare to the LES close to the exit of the chamber.

The gray gas emission intensity for different values of concentrations in PL = 3 is plotted in Figs. 8 and 9. The intensity at higher concentration values increases, and also, the obtained value is more consistent with Leckner [17] and Yin's [18] results. By comparing the three curves of Leckner [17] and Yin's [18] and the present results evidently show is in better agreement to Yin's and Leckner's model in comparison with LBL Model. Yin's [18] results have almost linear emission behavior over different temperatures. The results from the current study have a negligible difference in comparison with the Yin's model in which the concentration ratio is 2, an insignificant difference with Leckner's model in concentration ratio equal 0.125 for temperature larger than 900 K [17, 18]. Figure 10 illustrates the relationships among three essential factors namely temperature, total emissivity, and molar concentration. As to what has been shown, total emissivity decreases when the chamber's temperature increases; however, a rise in molar concentration in constant temperature increases emissivity. Thus, furnace's walls experience much more radiation when the chamber is experienced the transient heating state.

The variation of total emissivity in different temperature and path length pressure (PL) (Fig. 11) shows the importance of path length pressure variations in addition to temperature and molar concentration. Figure 11 provides complementary information to Fig. 10 in order to clarify other range of quantities that should be selected for either increase or decrease the level of total emissivity in a furnace to improve designing point ranges. As shown, the increase in path length pressure has a direct impact on total emissivity, and it in conjunction with other factors to shift the total emissivity to its peak. However, Fig. 10 shows that the molar concentration is key in raising the emissivity of the chamber; Fig. 11 provides much more accurate information

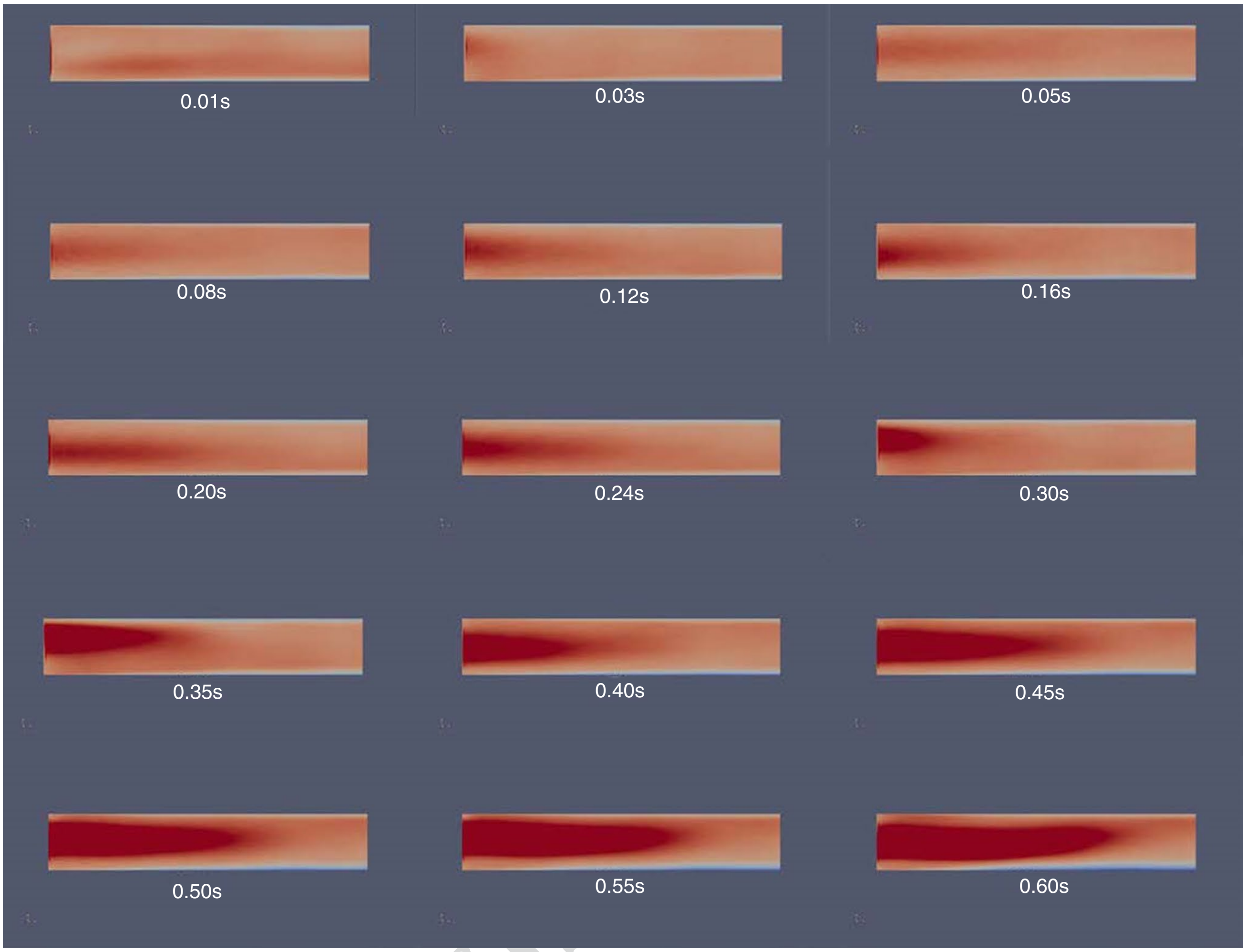

Fig. 4 Evolution of flame in different time periods

on this conclusion and shows that the dominant effects of the molar concentration changes are when its value stays under 2 mol. For values higher than 2 mol, minor fluctuations are presented, and thus it may be assume to be negligible.

As expected, the concentration of fuel decreases and water vapor increases during the combustion process (Figs. 12 and 13a). An elaborate survey on thermodynamic properties of the burning reaction reveals that burning CH_4 leads to energy production that is consumed for the phase-change process of H_2O and raising the temperature of products such as CO_2 and the combustion chamber. Figure 13b shows that the molar fraction of CO_2 increases during the combustion process. Figure 13b, the temperature inside the chamber increases when furnace consumes the fuel with a specific burning rate, and then the final temperature hits a peak value of 1700 K (Fig. 13c). Moreover, the wall heat flux experienced a steep rise add reaches the maximum amount of 30 kW/m^2 at $\frac{x}{L} = 0.8$ and then its value dropped to 27 kW/m^2 at the exit of chamber, in which the reduction of heat flux after reaching the maximum value shows the instability of flame may affect the heat flux behavior (Fig. 13d).

Figure 14 shows the radiant heat flux for gray gas and transparent gas assumptions for $\frac{2}{3} \le \frac{x}{L} \le 1$. The results show that assuming gray gas due to internal absorption energy in the combustion chamber leads to a more considerable amount than transparent gas. The results show that the impact is between 10 and 68%. The impact of considering radiation heat transfer for the combustion process is shown in Fig. 15. The simulation was carried out for two cases ie. heat flux with and without heat transfer due to radiation. The walls are consider as black, and the wall heat flux transferred from the gas to the wall will be equal to the heat flux removed from the wall. It can be seen that the impact

Journal : Large 10973	Article No : 10263	Pages : 18	MS Code : 10263	Dispatch : 24-1-2021

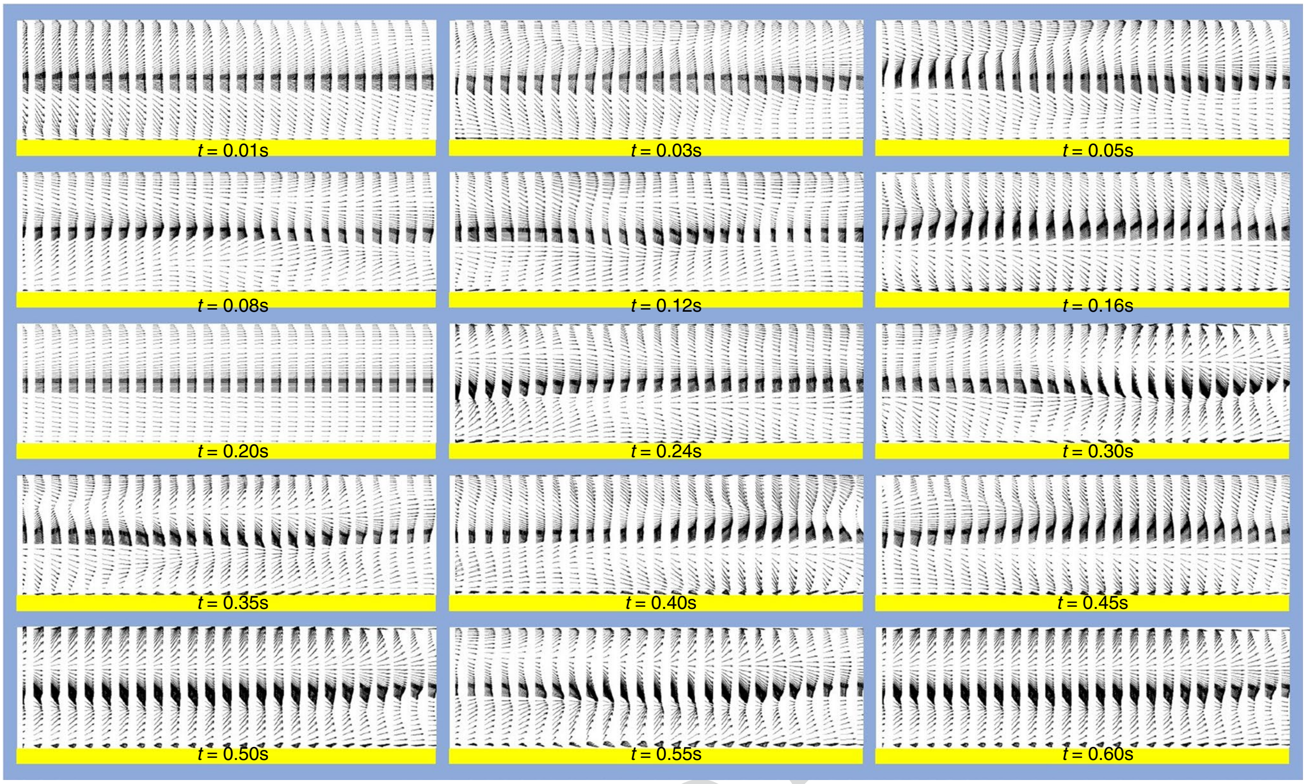

Fig. 5 Velocity vectors

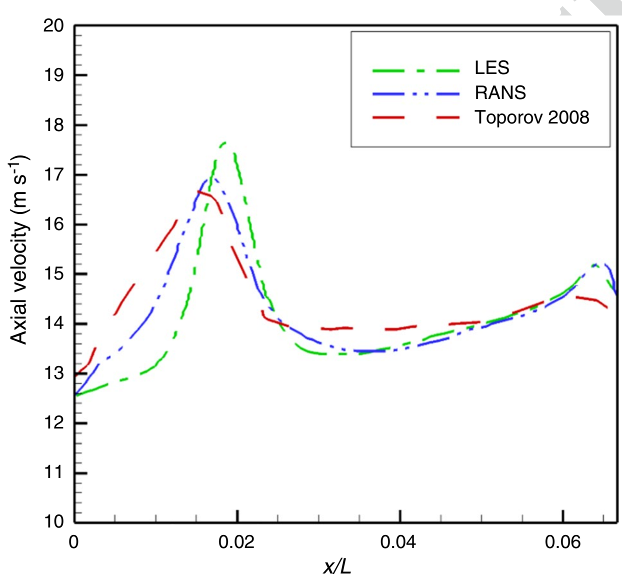

Fig. 6 Axial velocity distribution for different turbulence models ($0 < x/L < 0.067$)

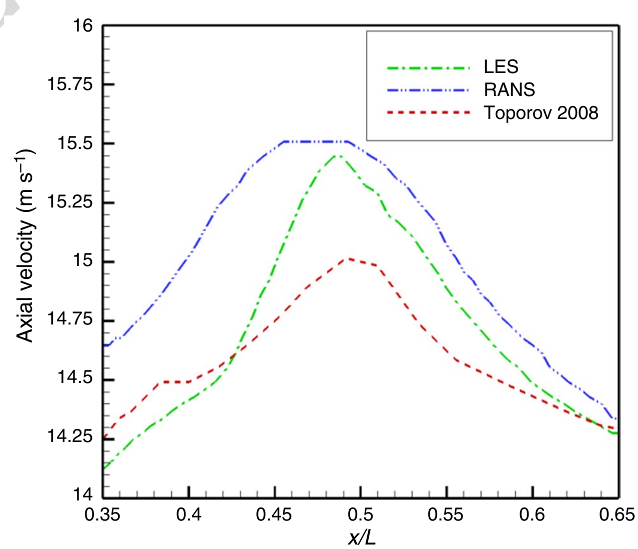

Fig. 7 Axial velocity distribution for different turbulence models ($0.33 < x/L < 0.67$)

of radiation heat transfer on the wall heat flux is between 10 and 40%.

Figure 16 shows that heat flux increases when the gas temperature increases during the combustion process. According to this figure, we can observe the effect of molar concentration and average emissivity. It can be concluded that the increase in average emissivity affects the heat flux at higher temperatures than at lower temperatures. For instance, the amount of heat flux in 800 K and

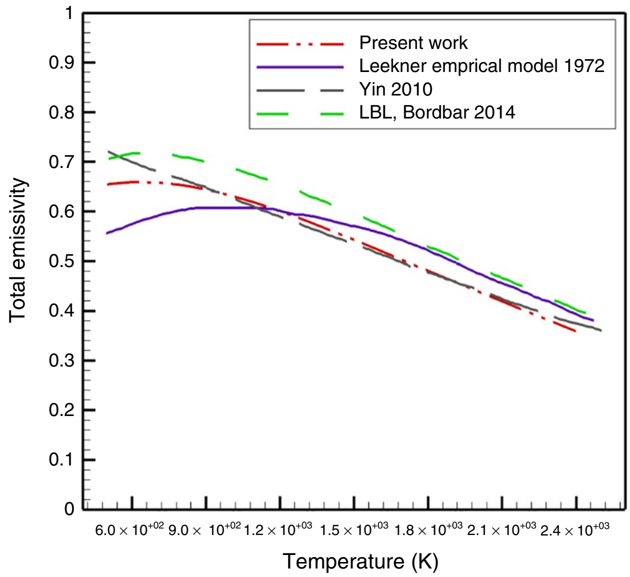

Fig. 8 Emission intensity obtained on the concentration ratio of 2

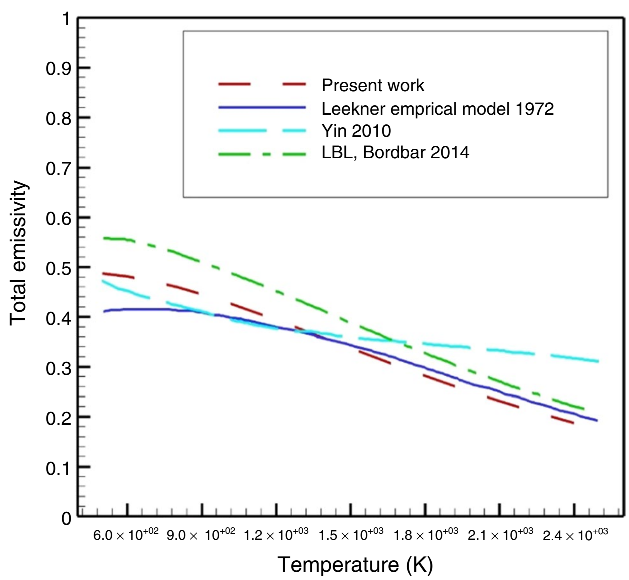

Fig. 9 Emission intensity obtained on the concentration ratio of 1/8

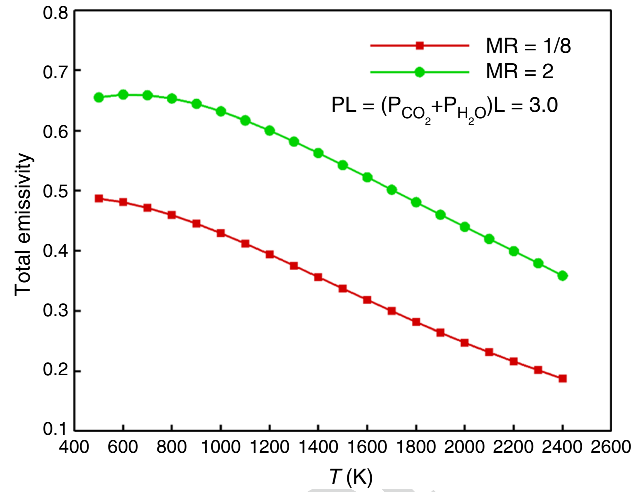

Fig. 10 Emission intensity obtained on MR = 1/8,2, and the pressure length of 3.0

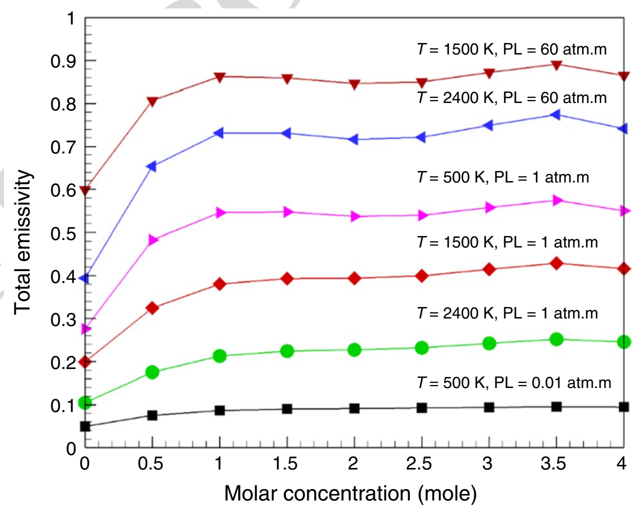

Fig. 11 Variation of total emissivity in different temperature and path length pressure (PL)

1400 K changes about 3 kW m^2 and 47 kW m^2 when the average emissivity varies from 0.3448 to 0.5385.

The type of fuel is one of the most critical factors in designing an efficient furnace. The ignition delay categorizes fuels from the point of view that engineers are able to use their desired fuel in order to manage the combustion duration, ignition interval times, etc. Figure 17 provides a detailed examination of two different fuels, by which the effect of temperature on ignition delays is measured. The Fig. 17 shows that the fuel ignition time increase much more rapidly with increasing time for CH_4 Methane compare to C_3H_8 Propane.

In this research, we examined the effect of an excessive amount of oxygen on turbulent viscosity and total heat flux. Figures 18 and 19 shows that a 27% increase in the amount of O_2, increase the turbulent viscosity and lowers the amount of total heat flux, respectively. This conclusion was we expected because a rise in oxidizer increases products such as vapor.

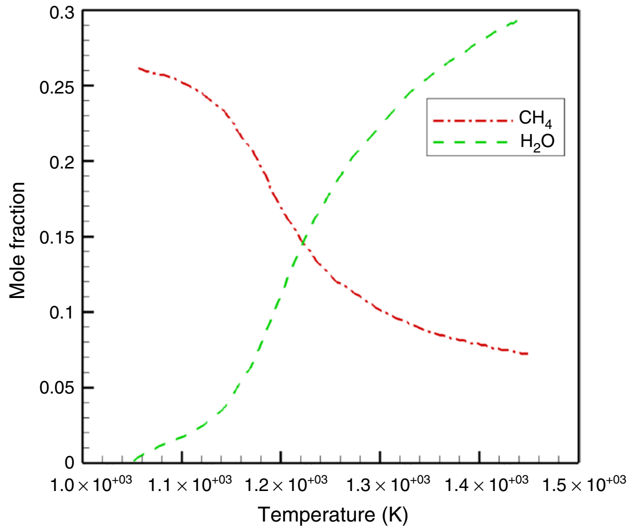

Fig. 12 Concentration variation of CH_4 and H_2O versus absolute temperature

Conclusions

The k-ε model was used for the initial condition for the RANS model, and the results of RANS were considered as the initial conditions for large eddy simulation. We then compared our results to existing literature to show the accuracy of LES model.

It is well known that excess oxygen percentage can significantly decrease the temperature of the combustion chamber because the excess oxygen leads to absorbing of the generated heat in the combustion process and, consequently, it reduces the temperature of the combustion chamber. The emission intensity value directly affects the amount of heat flux related to radiation heat transfer, and also combustion species concentration is directly related to the total emission intensity. The percentage of generated temperature due to the gas shows a convergence rate during the analysis with a surface temperature of the chamber. Regardless of heat transfer, the amount of heat generated is an integral part of the high-temperature heat transfer and is the heat transfer due to radiation. The gray gas limits the simulation only for atmospheric pressure but is more efficient for predicting both the different species and wide ranges of concentrations. The effect of radiation heat transfer with a gray-gas assumption on the wall heat flux and gas are between 10% to 68% and 10% to 40%, respectively. Therefore, the radiation heat transfer has a significant impact on the gas and wall heat flux and must be considered as a critical parameter.

It was found that the URANS (unsteady RANS) method does not model the fluid low behavior properly; therefore, turbulence have less effect on its solution. At the beginning of the numerical simulation, the implemented URANS method is more accurate than the LES model, but the LES model more accurate in evaluating large eddies and has ability to solve large scale, time and small scale properties.

Increases in the concentration of gases can directly affect the emission factor. On the other hand, the emission coefficient is proportional to the radiation heat transfer, and consequently, an increase in the concentration of gases increases the thermal radiation. Eventually, if the concentration of fuel or air is higher than the stoichiometric amount, some of the radiation energy is absorbed by excess fuel or air. Radiation heat transfer significantly depends on the environmental reaction. The assumption of transparent gas in order to obtain radiation from the radiation transmittance causes a significant deviation, and as a result, the calculated thermal flux differs significantly from the actual state, leading to in accurate determination of the temperature of the bulk and the wall temperature.

REVISED PROOF

Journal : Large 10973	Article No : 10263	Pages : 18	MS Code : 10263	Dispatch : 24-1-2021

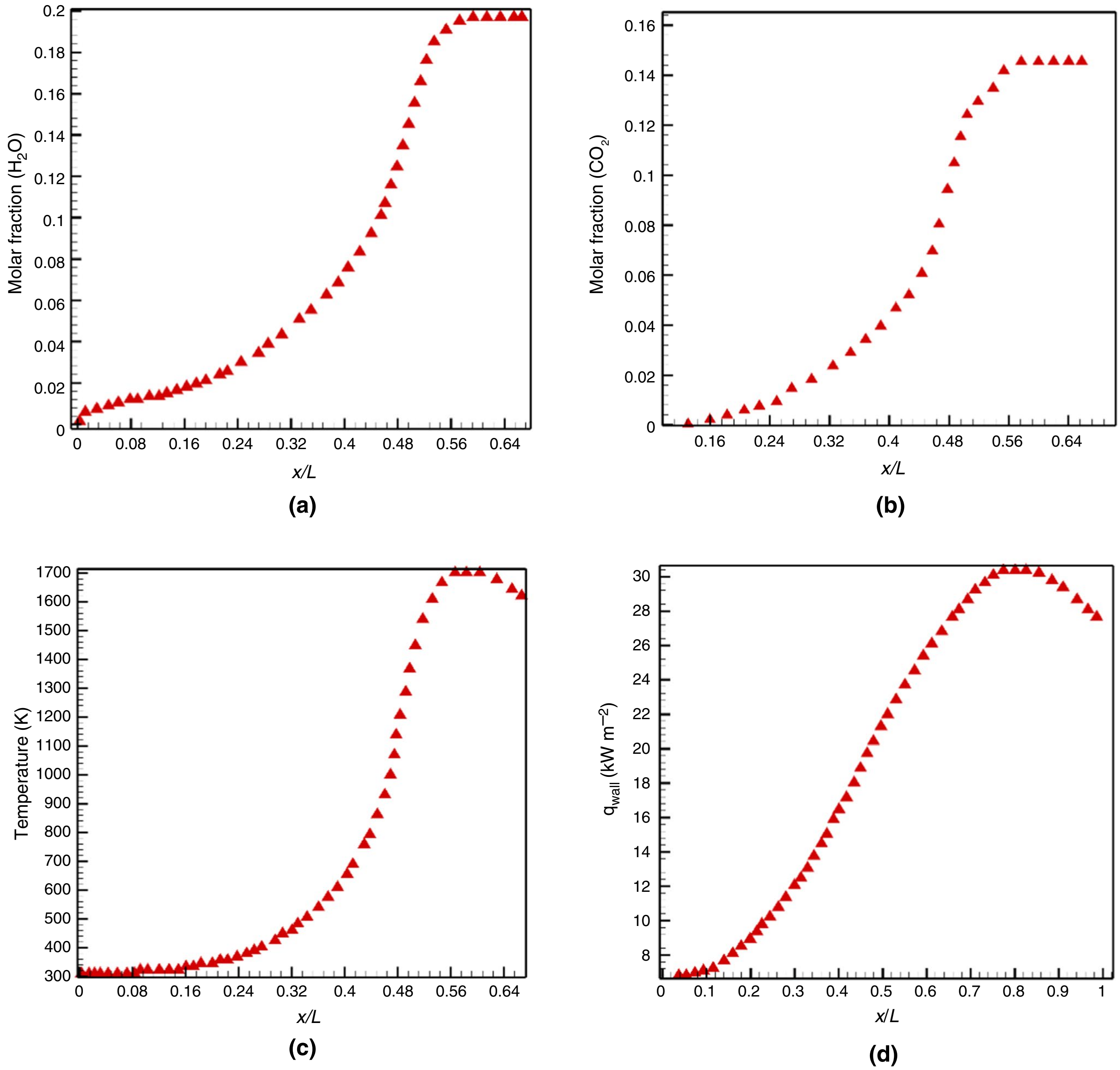

Fig. 13 The variation of different factors in the geometry. **a** Molar fraction of H_2O, **b** Molar fraction of CO_2, **c** Temperature, **d** Wall heat flux

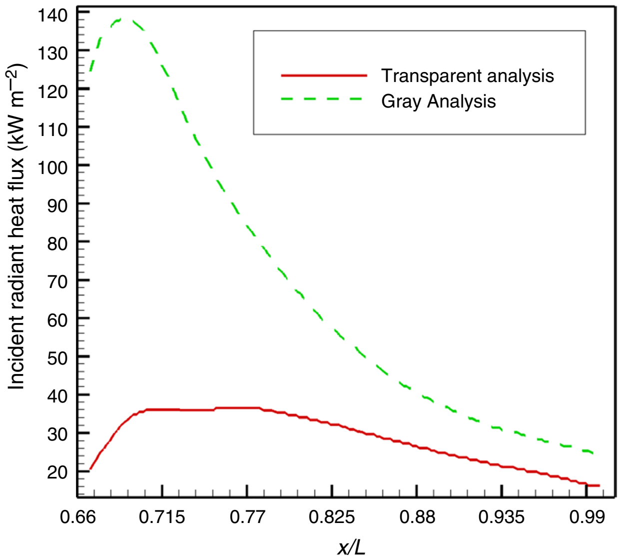

Fig. 14 Heat flux for two different gas environments for $\frac{2}{3} \leq \frac{x}{L} \leq 1$

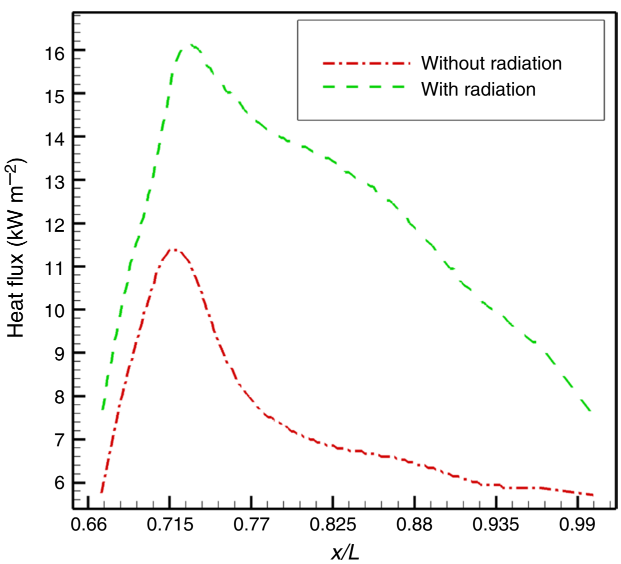

Fig. 15 Comparison of wall heat flux with and without heat transfer due to radiation for $\frac{2}{3} \leq \frac{x}{L} \leq 1$

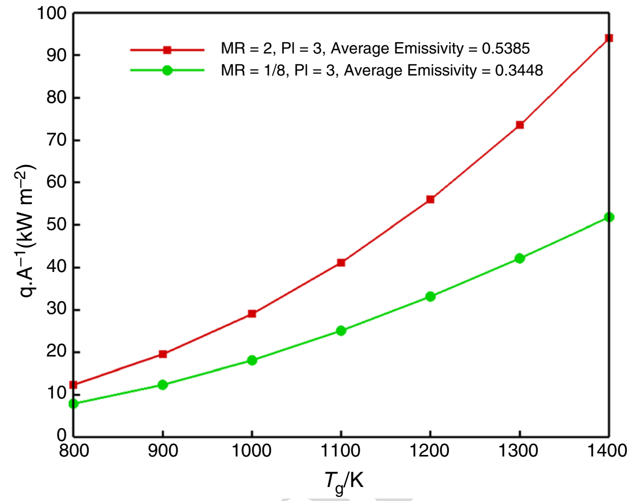

Fig. 16 The variation of heat flux with gas temperature and average emissivity changes

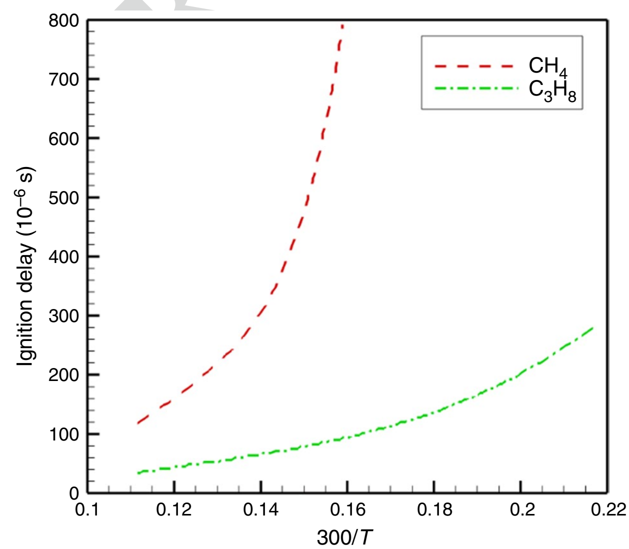

Fig. 17 Ignition delay for two different fuels

Journal : **Large 10973**	Article No : **10263**	Pages : **18**	MS Code : **10263**	Dispatch : **24-1-2021**

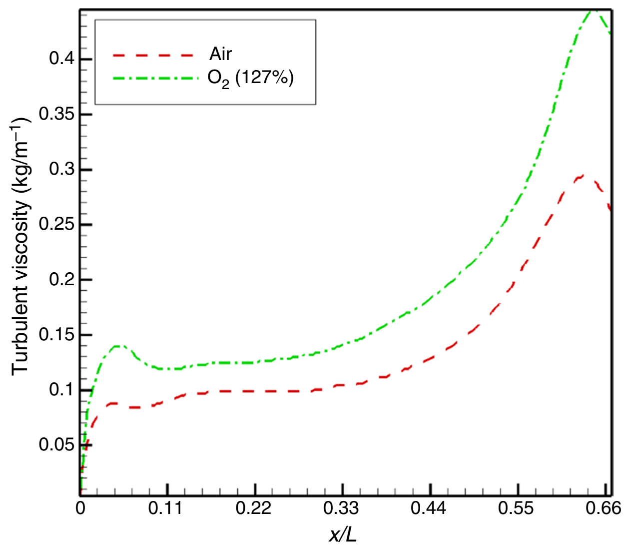

Fig. 18 The effect of excessive Oxygen on turbulent viscosity

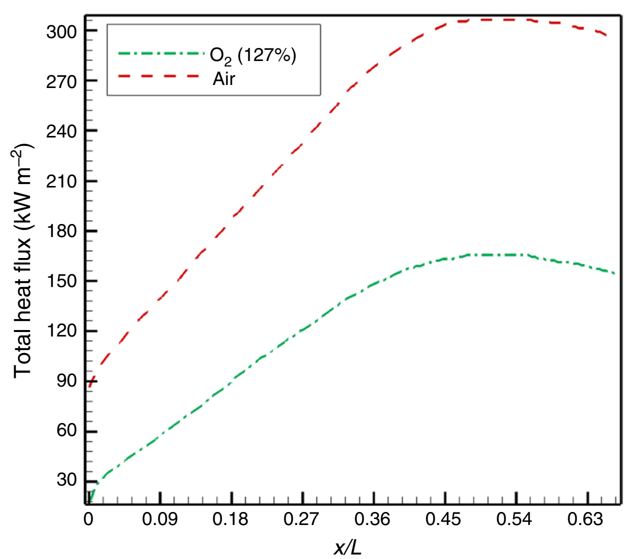

Fig. 19 The effect of excessive Oxygen on total heat flux

References

1. Fernandes R, Francis J. Combined conductive and radiative heat transfer in an absorbing, emitting, and scattering cylindrical medium. J Heat Transf. 1982;104:594–601.
2. Smith T, Shen Z, Friedman J. Evaluation of coefficients for the weighted sum of gray gases model. J Heat Transf. 1982;104:602–8.
3. Joo Peter H, Gigone Ben, Griffin Elizabeth A, Christensen Moah, Gülder Ömer L. Soot primary particle size dependence on combustion pressure in laminar ethylene diffusion flames. Fuel. 2018;220(15):464–70.
4. Lallemant N, Sayre A, Weber R. Evaluation of emissivity correlations for H_2O, CO_2, N_2/air mixtures and coupling with solution methods of the radiative transfer equation. Prog Energy Combust Sci. 1996;22:543–74.
5. Modest MF, Zhang H. The full-spectrum correlated-k distribution and its relationship to the weighted-sum-of-gray-gases method. ASME-Publications-Htd. 2000;366:75–84.
6. Li G, Modest MF. Application of composition PDF methods in the investigation of turbulence–radiation interactions. J Quant Spectrosc Radiat Transf. 2002;73:461–72.
7. Han CY. Radiative combustion of pyrolyzing fuel in a cylindrical combustor. Fuel. 2004;83:343–51.
8. Chen Z. Effects of radiation on large-scale spherical flame propagation. Combust Flame. 2017;183:66–74.
9. Wall T, Liu Y, Spero C, Elliott L, Khare S, Rathnam R, et al. An overview on oxyfuel coal combustion—state of the art research and technology development. Chem Eng Res Des. 2009;87:1003–16.
10. Hjärtstam S, Johansson R, Andersson K, Johnsson F. Computational fluid dynamics modelling of oxy-fuel flames: the role of soot and gas radiation. Energy Fuels. 2012;26:2786–97.
11. Ben-Mansour R, Habib M, Badr H, Nemitallah M. Characteristics of oxy-fuel combustion in an oxygen transport reactor. Energy Fuels. 2012;26:4599–606.
12. Centeno FR, da Silva CV, França FH. The influence of gas radiation on the thermal behavior of a 2D axisymmetric turbulent non-premixed methane–air flame. Energy Convers Manag. 2014;79:405–14.
13. Kuo KK. Principles of combustion. New York: Wiley; 1986.
14. Marshall S, Taylor SC, Davies T, Cracknell R. Laminar burning velocity measurements of liquid fuels at elevated pressures and temperatures with combustion residuals. Combust Flame. 2011;158:1920–32.
15. Cavaliere DE, Kariuki J, Mastorakos E. A comparison of the blow-off behaviour of swirl-stabilized premixed, non-premixed and spray flames. Flow Turbul Combust. 2013;91:347–72.
16. Turns SR. An introduction to combustion. New York: McGraw-Hill; 1996. p. 287.
17. Leckner B. Spectral and total emissivity of water vapor and carbon dioxide. Combust Flame. 1972;19:33–48.
18. Yin C, Johansen LC, Rosendahl LA, Kær SK. New weighted sum of gray gases model applicable to computational fluid dynamics (CFD) modelling of oxy–fuel combustion: derivation, validation, and implementation. Energy Fuels. 2010;24:6275–82.
19. Bordbar MH, Węcel G, Hyppänen T. A line by line based weighted sum of gray gases model for inhomogeneous CO_2–H_2O mixture in oxy-fired combustion. Combust Flame. 2014;161(9):2435–45.
20. Rothman LS, Gordon IE, Barber RJ, Dothe H, Gamache RR, Goldman A, Perevalov VI, Tashkun SA, Tennyson J. HITEMP, the high-temperature molecular spectroscopic database. J Quant Spectrosc Radiat Transf. 2010;111(15):2139–50.
21. Rivière P, Langlois S, Soufiani A, Taine J. An approximate data base of H2O infrared lines for high temperature applications at low resolution. Statistical narrow-band model parameters. J Quant Spectrosc Radiat Transf. 1995;53(2):221–34.
22. Chu H, Ren F, Wei Y. A comparison of two statistical narrow band models for non-gray gas radiation in planar plates. Therm Sci. 2018;22(Suppl 2):777–84.
23. Goody R. A statistical model for water vapour absorption. Q J R Meteorol Soc. 1952;78:165–9.
24. Malkmus W. Random Lorentz band model with exponential-tailed s-1 line intensity distribution function. J Opt Soc Am. 1967;57:323–9.
25. Toporov D, Bocian P, Heil P, Kellermann A, Stadler H, Tschunko S, Förster M, Kneer R. Detailed investigation of a pulverized fuel swirl flame in CO_2/O_2 atmosphere. Combust Flame. 2008;155(4):605–18.

26. Zhou Y, et al. Combustion of aluminum particles in a high-temperature furnace under various $O_2/CO_2/H_2O$ atmospheres. J Therm Anal Calorim. 2020;139(1):251–60.
27. Shanmukharadhya K, Sudhakar K. Experimental investigations for the location of reaction zones in a bagasse fired furnace. J Therm Anal Calorim. 2007;90(1):299–306.
28. Xiao Y, et al. Experimental study on the corresponding relationship between the index gases and critical temperature for coal spontaneous combustion. J Therm Anal Calorim. 2017;127(1):1009–17.
29. Ravangard AR, Momayez L, Rashidi M. Effects of geometry on simulation of two-phase flow in microchannel with density and viscosity contrast. J Therm Anal Calorim. 2020;139(1):427–40. https://doi.org/10.1007/s10973-019-08342.
30. H. Müller, F. Ferraro, M. Pfitzner, Implementation of a steady laminar flamelet model for nonpremixed combustion in LES and RANS simulations. In: Conference: 8th International OpenFOAM Workshop, At JeJu, Korea (2013).
31. Li Z, Sheikholeslami M, Chamkha AJ, Raizah ZA. Control volume finite element method for nanofluid MHD natural convective flow inside a sinusoidal annulus under the impact of thermal radiation. Comput Methods Appl Mech Eng. 2018;338:618–33.
32. Sheikholeslami M, Ghasemi A, Li Z, Shafee A, Saleem S. Influence of CuO nanoparticles on heat transfer behavior of PCM in solidification process considering radiative source term. Int J Heat Mass Transf. 2018;126:1252–64.
33. Sheikholeslami M, Jafaryar M, Saleem S, Li Z, Shafee A, Jiang Y. Nanofluid heat transfer augmentation and exergy loss inside a pipe equipped with innovative turbulators. Int J Heat Mass Transf. 2018;126(2018):156–63.
34. Ferchichi M, Tavoularis S. Scalar mixing and PDF in passively heated sheared turbulence. J Fluid Mech. 2002;461:155.

Publisher's Note Springer Nature remains neutral with regard to jurisdictional claims in published maps and institutional affiliations.

REVISED PROOF

Journal : **Large 10973**	Article No : **10263**	Pages : **18**	MS Code : **10263**	Dispatch : **24-1-2021**

View publication stats